
A geometric framework for momentum-based optimizers for low-rank training

Steffen Schotthöfer* Timon Klein† and Jonas Kusch‡

Abstract

Low-rank pre-training and fine-tuning have recently emerged as promising techniques for reducing the computational and storage costs of large neural networks. Training low-rank parameterizations typically relies on conventional optimizers such as heavy ball momentum methods or Adam. In this work, we identify and analyze potential difficulties that these training methods encounter when used to train low-rank parameterizations of weights. In particular, we show that classical momentum methods can struggle to converge to a local optimum due to the geometry of the underlying optimization landscape. To address this, we introduce novel training strategies derived from dynamical low-rank approximation, which explicitly account for the underlying geometric structure. Our approach leverages and combines tools from dynamical low-rank approximation and momentum-based optimization to design optimizers that respect the intrinsic geometry of the parameter space. We validate our methods through numerical experiments, demonstrating faster convergence, and stronger validation metrics at given parameter budgets.

1 Introduction

Deep learning models have achieved remarkable success across natural language processing and computer vision tasks, but their deployment remains computationally expensive due to the large number of trainable parameters. To address this, parameter-efficient strategies have been developed to reduce memory and compute requirements during training. Common approaches include sparsification [6, 19, 9], quantization [32, 4], and layer factorization. The latter has gained considerable attention for pre-training [31, 13, 24, 25, 36] and especially fine-tuning [12, 29, 37, 7, 38, 17, 23]. Layer factorization represents weights (or adapters) as low-rank matrices, allowing only the low-rank factors to be trained. This significantly reduces both memory usage and computational cost.

In the class of low-rank layer factorizations, one of the most popular methods is LoRA [12], which applied typical optimizers such as stochastic gradient descent (sgd) or Adaptive Moment Estimation (Adam) [14] directly to the low-rank factors. The combination of these optimizers with LoRA does not guarantee an optimal optimization trajectory [23, 37]. To overcome the former challenge, various improvements have been proposed: For example, LoRA+ [7] proposes the use of separate learning rates for different components of the low-rank decomposition, Dora [18] normalizes the factor matrices and introduces a magnitude parameter. Furthermore, to overcome the challenge of tuning the rank of the LoRA ansatz, AdaLoRA [37] adaptively allocating the parameter budget during training, by masking off rows and columns of the adapter matrices. Other low-rank methods focus entirely on the optimizer states: GaLore [38] projects full-rank weight gradients into a low-rank subspace to reduce the memory footprint of the optimizer state. Tensor-GaLore [5] generalizes this technique to high-order tensor-parameterized models, further improving efficiency for large-scale architectures.

*Computer Science and Mathematics Division; Oak Ridge National Laboratory; Oak Ridge, TN 37831 USA; Mail correspondence: schotthofers@ornl.gov

†Department of Mathematics; Otto-von-Guericke University Magdeburg; 39106; Magdeburg; Germany

‡Scientific Computing; Norwegian University of Life Sciences; Drøbakveien 31, 1433 Ås; Norway

Adafactor [27] approximates the second-moment matrix using a low-rank decomposition of Adam with low-rank factors.

A particularly promising class of layer factorization strategies is dynamical low-rank training (DLRT) which has been introduced in [24] and has since been used in various tasks [36, 25, 23, 3, 16]. DLRT projects the gradient flow dynamics onto the tangent space of the manifold of low-rank parameters, thereby achieving convergence guarantees to low-rank optimal weights [23]. However, these projections are inherently non-smooth, leading to ill-conditioned optimization landscapes and requiring smaller learning rates for stable training [24]. To ensure robust integration of such projections, DLRT constrains movement to flat subspaces within the low-rank manifold, enabling stable convergence to low-rank optima. The method is rank adaptive - using a basis augmentation and subsequent singular value-based truncation criterion to adapt the rank of the low-rank factorization. It further enables extensions to increase adversarial robustness of the compressed neural networks by enforcing orthonormality of the low-rank bases and projecting onto a well-conditioned manifold [22] or regularizing the condition number of the factor matrix [26].

Despite its efficiency, current DLRT approaches primarily rely on sgd, and it remains unclear how adaptive optimizers such as Adam [14] can be effectively applied. This is a significant limitation, as many state-of-the-art models depend on momentum-based optimizers like Adam and its variants for performance and stability. Therefore, the extension of DLRT to such optimization techniques is crucial.

To bridge this gap, we introduce a novel momentum-based optimization framework for low-rank pretraining and fine-tuning. The method integrates adaptive momentum techniques into the framework of dynamical low-rank training (DLRT), preserving the low-rank structure of model weights while enabling stable and efficient updates. This establishes a link between low-rank optimization and adaptive gradient methods, yielding both theoretical insights and practical improvements. Beyond the method derivation, we analyze why LoRA-style adapters—and low-rank parameterizations more broadly—require momentum-based optimizers that are aware of the geometry of the low-rank parameter space, i.e., the underlying manifold structure. Naively applying standard optimizers such as heavy ball to low-rank parameterizations can produce updates that do not correspond to a gradient flow leading to a low-rank optimum. As a result, these methods may fail to converge to valid low-rank solutions. We show how DLRT can be adapted to approximate geometry-respecting gradient flows that consistently drive convergence toward low-rank optima. Together, these contributions lay a foundation for more robust and efficient training of large-scale models under low-rank constraints.

Compared to low-rank methods that act on the optimizer states only [38, 5, 27] we provide a wholistic interpretation of a low-rank optimization algorithm that adaptively compresses the network weights, gradients and optimizer states simultaneously, achieving superior compression performance at high validation metrics. We remark that the method is directly extendable for tensor-valued neural networks using, e.g., low-rank Tucker factorization.

The paper is structured as follows: We first discuss limitations of naive momentum methods and show how to adapt the underlying gradient flow to achieve convergence to a low-rank optimum in Section 2. While the adapted gradient flow facilitates convergence, constructing robust numerical optimizers from it is challenging due to its inherent stiffness. We propose a low-rank heavy ball optimizer in Section 3 which integrates the adapted gradient flow robustly. In Section 4, we construct a fully low-rank Adam optimizer by leveraging insights gained in Section 3. In Section 5 we underline the efficiency of the proposed method through numerical experiments. In particular, we demonstrate fast convergence and superior validation accuracy at high compression levels for training from scratch, transfer learning, and low-rank finetuning of different neural network architectures and benchmarks.

2 Momentum-based low-rank training

We consider a low-rank neural network of the form

$$\mathcal{N}(x) = \sigma_L(U_L S_L V_L^\top z_{L-1}(x)),$$

where $z_{L-1}(x)$ is defined recursively by

$$z_0(x) = x \in \mathbb{R}^{n_0}, \quad \text{and} \quad z_l(x) = \sigma_l(U_l S_l V_l^\top z_{l-1}(x)) \in \mathbb{R}^{n_l}, \quad \forall l = 1, \dots, L. \quad (1)$$

Here, the weight matrices are defined as $W_l := U_l S_l V_l^\top \in \mathbb{R}^{n_l \times n_{l-1}}$, where $U_l \in \mathbb{R}^{n_l \times r_l}$ and $V_l \in \mathbb{R}^{n_{l-1} \times r_l}$ are orthonormal low-rank factors, and $S_l \in \mathbb{R}^{r_l \times r_l}$ is the coefficient matrix. Thus,

W_l lies in the manifold of rank r_l matrices which we denote by \mathcal{M}_{r_l} . Additionally, σ_l represents the activation function of layer l . For simplicity of notation, we do not consider biases, but a model with biases can always be expressed as (1) by folding biases into weights and creating an input dimension that is always one. Several methods have been proposed to train the low-rank weight matrices W_l to minimize a given loss function \mathcal{L} . Among these, the simplest training rule is the steepest descent method, which, for a fixed⁴ layer l with weights $W = USV^\top \equiv W_l$ reads

$$U^{n+1} = U^n - \lambda \nabla_U \mathcal{L}^n, \quad S^{n+1} = S^n - \lambda \nabla_S \mathcal{L}^n, \quad V^{n+1} = V^n - \lambda \nabla_V \mathcal{L}^n, \quad (2)$$

where λ is the learning rate, the index n denotes the training iteration, and we have used the shorthand notation $\mathcal{L}^n := \mathcal{L}(U^n S^n V^{n,\top})$. A more general framework that facilitates the numerical analysis and construction of novel numerical methods interprets the steepest descent method as an explicit Euler time discretization of the continuous gradient flow equations

$$\dot{U}(t) = -\nabla_U \mathcal{L}, \quad \dot{S}(t) = -\nabla_S \mathcal{L}, \quad \dot{V}(t) = -\nabla_V \mathcal{L},$$

where $\mathcal{L} := \mathcal{L}(U(t)S(t)V(t)^\top)$. Then, the steepest descent update equation for the individual factors can be obtained through a forward Euler discretization of the pseudo-time t . E.g., the update equation for U can be retrieved through $\dot{U}(t_n) \approx \frac{1}{\lambda}(U^{n+1} - U^n)$ and $\mathcal{L} \approx \mathcal{L}^n$. While steepest descent methods offer a simple strategy to drive the parameters to a locally optimal point, one of the most widely adopted strategies for updating factorized parameters W , along with their factorized momentum terms $\mathcal{V} = U_V S_V V_V^\top$, involves momentum-based optimization. For instance, in the case of the heavy ball method applied to all low-rank factors individually, e.g., in LoRA [12], the associated update equations take the form

$$U^{n+1} = U^n + \lambda U_V^n, \quad U_V^{n+1} = (1 - \lambda\gamma) U_V^n - \lambda \nabla_U \mathcal{L}^n, \quad \nabla_U \mathcal{L}^n = (\nabla_W \mathcal{L}^n) V^n (S^n)^\top, \quad (3a)$$

$$V^{n+1} = V^n + \lambda V_V^n, \quad V_V^{n+1} = (1 - \lambda\gamma) V_V^n - \lambda \nabla_V \mathcal{L}^n, \quad \nabla_V \mathcal{L}^n = (\nabla_W \mathcal{L}^n)^\top U^n S^n, \quad (3b)$$

$$S^{n+1} = S^n + \lambda S_V^n, \quad S_V^{n+1} = (1 - \lambda\gamma) S_V^n - \lambda \nabla_S \mathcal{L}^n, \quad \nabla_S \mathcal{L}^n = (U^n)^\top (\nabla_W \mathcal{L}^n) V^n. \quad (3c)$$

The associated gradient flow equations are given by:

$$\dot{U} = U_V, \quad \dot{U}_V + \gamma U_V + \nabla_U \mathcal{L} = 0, \quad \nabla_U \mathcal{L} = (\nabla_W \mathcal{L}) V S^\top, \quad (4a)$$

$$\dot{V} = V_V, \quad \dot{V}_V + \gamma V_V + \nabla_V \mathcal{L} = 0, \quad \nabla_V \mathcal{L} = (\nabla_W \mathcal{L})^\top U S, \quad (4b)$$

$$\dot{S} = S_V, \quad \dot{S}_V + \gamma S_V + \nabla_S \mathcal{L} = 0, \quad \nabla_S \mathcal{L} = U^\top \nabla_W \mathcal{L} V. \quad (4c)$$

While these equations are optimal when treating all low-rank factors in isolation, they do not account for the fact that factors change simultaneously. For example, (4a) is expected to drive the solution to an optimum, only if $S(t)$ and $V(t)$ remain constant in time. When accounting for the dynamics of all three low-rank factors, the resulting gradient flow for $W(t) = U(t)S(t)V(t)^\top$ takes the form

$$\begin{aligned} \dot{W} &= U_V S V^\top + U S_V V^\top + U S V_V^\top, \quad \text{and} \\ \dot{\mathcal{V}} + 3\gamma \mathcal{V} &= -\nabla_U \mathcal{L} S_V V_V^\top - U_V \nabla_S \mathcal{L} V_V^\top - U_V S_V \nabla_V \mathcal{L}^\top \\ &= -(\nabla_W \mathcal{L}) V S^\top S_V V_V^\top - U_V U^\top \nabla_W \mathcal{L} V V_V^\top - U_V S_V S^\top U^\top \nabla_W \mathcal{L} \\ &=: -\hat{P}(W, \mathcal{V}) \nabla_W \mathcal{L}. \end{aligned}$$

This can easily be shown with the product rule, e.g., $\dot{W} = \dot{U} S V^\top + U \dot{S} V^\top + U S \dot{V}^\top$ and plugging in time derivatives from (4). These evolution equations for W and \mathcal{V} are fundamentally different from the momentum-based gradient flow equations of the full-rank problem

$$\dot{W}_{\text{full}} = \mathcal{V}_{\text{full}}, \quad \dot{\mathcal{V}}_{\text{full}} + \gamma \mathcal{V}_{\text{full}} = -\nabla_W \mathcal{L}(W_{\text{full}}). \quad (5)$$

Indeed, a proper formulation of (5) that drives the weights of a heavy ball method to a local optimum while preserving the low-rank representation of W , requires that

$$\dot{W} = P(W) \mathcal{V}, \quad \dot{\mathcal{V}} + \gamma \mathcal{V} = -P(W) \nabla_W \mathcal{L}, \quad (6)$$

where for $W = U S V^\top$, the projector onto the tangent space is given by $P(W)Z := U U^\top Z (I - V V^\top) + Z V V^\top$, see [15, Lemma 4.1] and Figure 1 for geometric interpretation. Note that in

⁴We restrict the discussion to a single layer without loss of generality, following the arguments of [23, Appendix I].

abuse of notation, we have recycled W and \mathcal{V} here to denote the weights and momentum terms following equation (6) instead of the naive equations (4). Then, the time evolution will drive W into a low-rank steady state (W^*, \mathcal{V}^*) such that $P(W^*)\nabla_W \mathcal{L}(W^*) = 0$, see Theorem 1. This steady state thus fulfills the optimality condition of a local optimum, see, e.g. [21]. Such a condition is not ensured by the simultaneous descent equations of (4) since, in general, $\dot{W} \neq P(W)\mathcal{V}$ and $\widehat{P}(W, \mathcal{V})\nabla_W \mathcal{L} \neq P(W)\nabla_W \mathcal{L}$. Therefore, training low-rank factors with conventional momentum methods does not necessarily ensure convergence to a low-rank optimum.

We aim to derive a numerical method that is consistent with the optimal gradient-flow equations (6). A central limitation of (6) is that it does not preserve the low-rank structure of the momentum term \mathcal{V} , thus leading to prohibitive computational costs and memory requirements. Instead, we aim to derive a method that fulfills

$$\dot{\mathcal{V}} + \gamma\mathcal{V} = -P(\mathcal{V})\nabla_W \mathcal{L} \quad (7)$$

which preserves the low-rank structure of the momentum term. Indeed, the factorized solution of (7) fulfills (see Theorem 2)

$$\dot{U}_{\mathcal{V}} = -(I - U_{\mathcal{V}}U_{\mathcal{V}}^{\top})\nabla_W \mathcal{L}V_{\mathcal{V}}S_{\mathcal{V}}^{-1}, \quad (8a)$$

$$\dot{V}_{\mathcal{V}} = -(I - V_{\mathcal{V}}V_{\mathcal{V}}^{\top})\nabla_W \mathcal{L}^{\top}U_{\mathcal{V}}S_{\mathcal{V}}^{-\top}, \quad (8b)$$

$$\dot{S}_{\mathcal{V}} = -\gamma S_{\mathcal{V}} - U_{\mathcal{V}}^{\top}\nabla_W \mathcal{L}V_{\mathcal{V}}, \quad (8c)$$

with initial condition $U(0) = U_{\mathcal{V}}(0)$ and $V(0) = V_{\mathcal{V}}(0)$. While this formulation and in particular (6) provide a good basis for constructing numerical methods, it also introduces the inverse terms $S_{\mathcal{V}}^{-1}$ and $S_{\mathcal{V}}^{-\top}$ on the right-hand side, rendering the system highly stiff, especially when these matrices are ill-conditioned. This stiffness can be treated through robust time integrators [1, 2] developed in the field of dynamical low-rank approximation [15] which have also been used for stochastic-gradient descent methods in dynamical low-rank training [24, 36, 25, 23, 10, 26]. In the following section, we formulate an algorithm that provably approximates the gradient flow (8) by following ideas of [1]. It turns out that this method is a consistent approximation of the optimal gradient flow (6) under mild assumptions.

3 A low-rank heavy ball method

To approximate (6), we start with the first time step from $t_0 = 0$ to $t_1 = \lambda$ and note that by definition of the initial condition $U^0 := U(t_0) = U_{\mathcal{V}}(t_0)$ and $V^0 := V(t_0) = V_{\mathcal{V}}(t_0)$. Let us first construct an augmented basis to ensure that the range and co-range of \mathcal{V} are fully spanned. To ensure robustness to small singular values, we introduce a change of variables and evolve the basis along $K_{\mathcal{V}}(t) = U_{\mathcal{V}}(t)S_{\mathcal{V}}(t)$ and $L_{\mathcal{V}}(t) = V_{\mathcal{V}}(t)S_{\mathcal{V}}(t)^{\top}$ for $t \in [t_0, t_1]$ while keeping $V^0 = V_{\mathcal{V}}(t_0)$ and $U^0 = U_{\mathcal{V}}(t_0)$ fixed, respectively [1]. Then, using the product rule and derivatives from (8), we get

$$\begin{aligned} \dot{K}_{\mathcal{V}}(t) &= \dot{U}_{\mathcal{V}}(t)S_{\mathcal{V}}(t) + U_{\mathcal{V}}(t)\dot{S}_{\mathcal{V}}(t) \stackrel{(8)}{=} -\nabla_W \mathcal{L}(W(t))V^0, & K_{\mathcal{V}}(t_0) &= U^0S_v^0, \\ \dot{L}_{\mathcal{V}}(t) &= \dot{V}_{\mathcal{V}}(t)S_{\mathcal{V}}(t)^{\top} + V_{\mathcal{V}}(t)\dot{S}_{\mathcal{V}}(t)^{\top} \stackrel{(8)}{=} -\nabla_W \mathcal{L}(W(t))^{\top}U^0, & L_{\mathcal{V}}(t_0) &= V^0S_v^{0,\top}. \end{aligned}$$

As no ill-conditioned $S_{\mathcal{V}}^{-1}$ terms affect the dynamics, one can use a forward Euler step to update $K_{\mathcal{V}}$ and $L_{\mathcal{V}}$ from t_0 to the next time step t_1 . Thus, we get for $K_{\mathcal{V}}^n \approx K_{\mathcal{V}}(t_n)$, $L_{\mathcal{V}}^n \approx L_{\mathcal{V}}(t_n)$, and $W^n = W(t_n)$

$$\begin{aligned} K_{\mathcal{V}}^1 &= K_{\mathcal{V}}^0 - \lambda \nabla_W \mathcal{L}(W^0)V^0, & \text{with } K_{\mathcal{V}}^0 &= U^0S_v^0, \\ L_{\mathcal{V}}^1 &= L_{\mathcal{V}}^0 - \lambda \nabla_W \mathcal{L}(W^0)^{\top}U^0, & \text{with } L_{\mathcal{V}}^0 &= V^0S_v^{0,\top}. \end{aligned}$$

Denoting an orthonormalization algorithm like Gram-Schmidt as ortho , $K_{\mathcal{V}}^1$ and $L_{\mathcal{V}}^1$ are therefore spanned by

$$\widehat{U} = \text{ortho}(U^0, \nabla_W \mathcal{L}(W^0)V^0), \quad \widehat{V} = \text{ortho}(V^0, (\nabla_W \mathcal{L}(W^0))^{\top}U^0).$$

Following [35, Cor. 2.2], we note that $\nabla_U \mathcal{L} = \nabla_W \mathcal{L}V S^{\top}$ and $\nabla_V \mathcal{L} = (\nabla_W \mathcal{L})^{\top}U S$, meaning that \widehat{U} and \widehat{V} can be rewritten as

$$\widehat{U} = \text{ortho}(U^0, \nabla_U \mathcal{L}(W^0)), \quad \widehat{V} = \text{ortho}(V^0, \nabla_V \mathcal{L}(W^0)).$$

We note here that this choice of the updated bases for \mathcal{V} also approximates the updated parameters $W(t_1)$ of the equation $\dot{W} = \mathcal{V}$. With an implicit Euler time discretization, we have

$$W^1 = U^0 S^0 V^{0,\top} + \lambda \hat{U} \hat{S}_\mathcal{V}^1 \hat{V}^\top = \hat{U} (\hat{U}^\top U^0 S^0 V^{0,\top} \hat{V} + \lambda \hat{S}_\mathcal{V}^1) \hat{V}^\top =: \hat{U} \hat{S}^1 \hat{V}^\top,$$

where $\hat{S}^1 := \hat{U}^\top U^0 S^0 V^{0,\top} \hat{V} + \lambda \hat{S}_\mathcal{V}^1$ and $\hat{S}_\mathcal{V}^1$ is the time-updated coefficient matrix of \mathcal{V} which we will derive in the following: Solving (8c) with fixed bases \hat{U} and \hat{V} yields

$$\dot{S}_\mathcal{V}(t) = -\gamma S_\mathcal{V}(t) - \hat{U}^\top \nabla_W \mathcal{L}(W(t)) \hat{V} \quad S_\mathcal{V}(t_0) = \hat{U}^\top U^0 S^0 V^{0,\top} \hat{V}.$$

Here, we choose $S_\mathcal{V}(t_0)$ as the coefficient matrix $S_\mathcal{V}^0$ projected to the updated bases \hat{U} and \hat{V} . This choice is crucial as it ensures the momentum term to be spanned with the updated basis. Using a forward Euler time discretization yields

$$\hat{S}_\mathcal{V}^1 = (1 - \gamma) \hat{U}^\top U^0 S^0 V^{0,\top} \hat{V} - \lambda \hat{U}^\top \nabla_W \mathcal{L}(U^0 S^0 V^{0,\top}) \hat{V}.$$

Let us note that with $\bar{S} := \hat{U}^\top U^0 S^0 V^{0,\top} \hat{V}$ we have

$$\hat{U}^\top \nabla_W \mathcal{L}(U^0 S^0 V^{0,\top}) \hat{V} = \nabla_{\bar{S}} \mathcal{L}(\hat{U} \bar{S} \hat{V}^\top).$$

Thus, with $\bar{S}_\mathcal{V} := \hat{U}^\top U^0 S_\mathcal{V}^0 V^{0,\top} \hat{V}$, the final coefficient updates (including the update for S) are

$$\begin{aligned} \hat{S}_\mathcal{V}^1 &= (1 - \gamma) \bar{S}_\mathcal{V} - \lambda \nabla_{\bar{S}} \mathcal{L}(\hat{U} \bar{S} \hat{V}^\top) \\ \hat{S}^1 &= \bar{S} + \lambda \hat{S}_\mathcal{V}^1. \end{aligned}$$

We note that the basis for W and \mathcal{V} remain identical after one time update, thus the above derivation holds for general time updates from t_n to t_{n+1} . Since, by construction, the updated bases \hat{U} and \hat{V} have doubled in rank compared to U^n and V^n , we perform a truncation step. The truncation can be performed back to the original rank r , or formulated with a relative truncation threshold for a given tolerance parameter $\vartheta = \tau \|\hat{S}\|$ [1] or a rank budget [37], enabling a rank adaptive method.

One step of the resulting method using a relative truncation threshold is summarized in Algorithm 1. A main distinction of this method from a naive application of a heavy ball method to DLRT [24] is that 1) our method uses the same bases for parameters and momentum terms, 2) our method does not use a momentum method to update the bases, but uses a classical basis augmentation instead, and 3) the method projects momentum terms onto the new bases after the basis update. These three choices ensure that the method approximates the optimal gradient flow (6) independent of the condition number of S^{-1} and $S_\mathcal{V}^{-1}$ when the truncation tolerance is sufficiently small, which we make rigorous in Theorem 3.

Theorem 3 shows that the low-rank momentum method produces solutions that are close to the solutions of full-rank (baseline) trained neural networks. Thus, we expect the validation accuracy of the trained low-rank networks to match the full-rank baseline. This is empirically confirmed in Table 1.

4 A low-rank Adam method

While heavy ball methods are the cornerstone of momentum-based optimization, they are commonly outperformed by momentum-based optimization methods that include stepsize control. Among these,

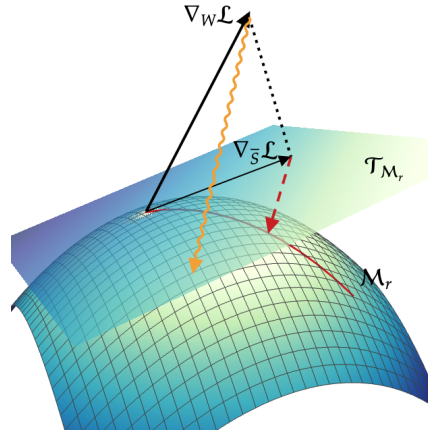


Figure 1: Geometric interpretation of Algorithm 1. First, we compute the parametrization of the tangent plane $\mathcal{T}_{\mathcal{M}_r}$. Then we compute the projected gradient $\nabla_{\bar{S}} \mathcal{L}$ to construct the low-rank momentum update. The momentum optimizer is subsequently applied to the low-rank weight coefficient \hat{S} . Lastly, we retract the updated coefficients back onto the manifold \mathcal{M}_r . The interpretation of Algorithm 2 is analogous. LoRA-like methods do not employ orthogonal projections onto $\mathcal{T}_{\mathcal{M}_r}$, but instead map the full gradient $\nabla_W \mathcal{L}$ implicitly onto \mathcal{M}_r . The linear map (displayed as the wavy orange line) may map the gradient direction far away from the properly projected gradient flow, leading to sub-optimal descent directions.

Algorithm 1: Single iteration of the dynamical low-rank momentum method.

The functions `basis_augmentation`, and `truncation` are detailed in Algorithm 3 in the appendix.

Input : Initial orthonormal bases $U, V \in \mathbb{R}^{n \times r}$ and coefficients $S, S_V \in \mathbb{R}^{r \times r}$;

τ : singular value threshold for rank truncation;

λ : learning rate.

- 1 Evaluate $\mathcal{L}(USV^\top)$ /* Forward evaluate */
 - 2 $G_U \leftarrow \nabla_U \mathcal{L}(USV^\top)$; $G_V \leftarrow \nabla_V \mathcal{L}(USV^\top)$ /* Backprop */
 - 3 $\begin{cases} \hat{U} \leftarrow \text{basis_augmentation}(U, G_U) \\ \hat{V} \leftarrow \text{basis_augmentation}(V, G_V) \end{cases}$ /* in parallel */
 - 4 $\bar{S} \leftarrow \hat{U}^\top USV^\top \hat{V}$; $\bar{S}_V \leftarrow \hat{U}^\top US_V V^\top \hat{V}$
 - 5 Evaluate $\mathcal{L}(\hat{U} \bar{S} \hat{V}^\top)$ /* Forward evaluate */
 - 6 $G_S \leftarrow \nabla_{\bar{S}} \mathcal{L}(\hat{U} \bar{S} \hat{V}^\top)$ /* Backprop */
 - 7 $\hat{S}_V \leftarrow (1 - \gamma) \bar{S}_V - \lambda G_S$; $\hat{S} \leftarrow \bar{S} + \lambda \hat{S}_V$ /* coefficient update */
 - 8 $U, S, V, S_V \leftarrow \text{truncation}(\hat{S}, \hat{S}_V, \hat{U}, \hat{V}; \tau)$
-

perhaps the most popular method is Adaptive Moment Estimation (Adam), which was introduced in [14] and has significantly impacted the machine learning community; see Algorithm 4 for a reference formulation of Adam. While Adam exhibits superior performance, the non-linearities it introduces and a missing gradient flow formulation make a rigorous derivation of an extension to LoRA-type training difficult. In the following, we use the insights gained from the heavy ball method to construct a low-rank Adam optimizer. Adam’s main distinction from heavy ball methods is the adaptive stepsize control, which is determined from the exponentially weighted moving average of the first and second moment of the gradient, denoted by \mathcal{V} and \mathcal{K} .

A naive update of the exponentially weighted moving average of the first and second moment of the gradients with respect to the coefficients S , which we denote as $\mathcal{V}_S, \mathcal{K}_S \in \mathbb{R}^{2r \times 2r}$ would read as

$$\mathcal{V}_S^{n+1} = \beta_1 \mathcal{V}_S^n + (1 - \beta_1) \nabla_S \mathcal{L} \quad \text{and} \quad \mathcal{K}_S^{n+1} = \beta_2 \mathcal{K}_S^n + (1 - \beta_2) (\nabla_S \mathcal{L})^2.$$

The bases U, V of the weight factorization could be updated as in Algorithm 1. However, this naive approach does not account for the fact that \mathcal{K}_S^n and \mathcal{K}_S^{n+1} , respectively \mathcal{V}_S^n and \mathcal{V}_S^{n+1} belong to different bases, who are updated between optimization steps by the augmentation-truncation mechanic.

Instead, we leverage the discussion in Section 3, and propose to project the previous weighted moving average to the updated bases. We note that through the construction of the low-rank bases, no step-size control is required to update U and V since the basis spans weights and moments at the old and current time steps and linear combinations in between. To facilitate the discussion, we denote the first low-rank moment as $S_V \in \mathbb{R}^{r \times r}$, analogously to the momentum term in Algorithm 1 and note that the update of S_V can be performed using the strategy of Algorithm 1 with $\bar{S}_V := \hat{U}^\top U^0 S_V^0 V^{0, \top} \hat{V}$ and $\bar{S} := \hat{U}^\top U^0 S^0 V^{0, \top} \hat{V}$, i.e.,

$$\hat{S}_V^1 = \beta_1 \bar{S}_V + (1 - \beta_1) \nabla_{\bar{S}} \mathcal{L}(\hat{U} \bar{S} \hat{V}^\top)$$

The dynamics of the second moment do not follow the gradient flow directly, but have non-linear dynamics depending on the square of the gradient. We remark that, the (full-rank) second moment $\hat{\mathcal{K}}$ is element-wise positive, which is important for taking the square root in the (full-rank) Adam update step $W^{n+1} = W^n - \lambda \frac{\hat{\mathcal{V}}}{\sqrt{\hat{\mathcal{K}} + \epsilon}}$. Denoting the second moment of the coefficient matrix by $S_K \in \mathbb{R}^{r \times r}$,

we propose a modified projection $\bar{S}_K = \left(\hat{U}^\top U^0 \sqrt{S_K^0} V^{0, \top} \hat{V} \right)^2$, which projects the element-wise square root of the second moment of the low-rank coefficient S onto the new basis and subsequently squares the elements. This ensures element-wise positivity of the second low-rank moment. The augmented low-rank moment \bar{S}_K is subsequently updated with the standard Adam update scheme

$$\hat{S}_K^1 = \beta_2 \bar{S}_K + (1 - \beta_2) \left(\nabla_{\bar{S}} \mathcal{L}(\hat{U} \bar{S} \hat{V}^\top) \right)^2.$$

Algorithm 2: Single iteration of the low-rank Adam method.

The functions `basis_augmentation`, and `truncation` are detailed in 3 in the appendix.

Input : Initial orthonormal bases $U, V \in \mathbb{R}^{n \times r}$ and coefficients $S, S_{\mathcal{V}}, S_{\mathcal{K}} \in \mathbb{R}^{r \times r}$;

τ : singular value threshold for rank truncation;

λ : learning rate;

β_1, β_2 : Adam momentum parameters;

ϵ : Small stability constant.

```

1 Evaluate  $\mathcal{L}(USV^\top)$  /* Forward evaluate */
2  $G_U \leftarrow \nabla_U \mathcal{L}(USV^\top); G_V \leftarrow \nabla_V \mathcal{L}(USV^\top)$  /* Backprop */
3  $\begin{cases} \hat{U} \leftarrow \text{basis\_augmentation}(U, G_U) \\ \hat{V} \leftarrow \text{basis\_augmentation}(V, G_V) \end{cases}$  /* in parallel */
4  $\bar{S} \leftarrow \hat{U}^\top USV^\top \hat{V}, \bar{S}_{\mathcal{V}} \leftarrow \hat{U}^\top US_{\mathcal{V}} V^\top \hat{V}, \bar{S}_{\mathcal{K}} \leftarrow \left( \hat{U}^\top U \sqrt{S_{\mathcal{K}}} V^\top \hat{V} \right)^2$ 
5 Evaluate  $\mathcal{L}(\hat{U} \bar{S} \hat{V}^\top)$  /* Forward evaluate */
6  $G_S \leftarrow \nabla_{\bar{S}} \mathcal{L}(\hat{U} \bar{S} \hat{V}^\top)$  /* Backprop */
7  $\hat{S}_{\mathcal{V}} \leftarrow \beta_1 \bar{S}_{\mathcal{V}} + (1 - \beta_1) G_S$ 
8  $\hat{S}_{\mathcal{K}} \leftarrow \beta_2 \bar{S}_{\mathcal{K}} + (1 - \beta_2) (G_S)^2$ 
  ▷ Modifications for adaptive update
9  $\check{S}_{\mathcal{V}} \leftarrow \frac{\hat{S}_{\mathcal{V}}^n}{1 - \beta_1^n}, \check{S}_{\mathcal{K}} \leftarrow \frac{\hat{S}_{\mathcal{K}}^n}{1 - \beta_2^n}$  /* Bias correction */
10  $\hat{S}^1 \leftarrow \bar{S} - \lambda \frac{\check{S}_{\mathcal{V}}}{\sqrt{\hat{S}_{\mathcal{K}} + \epsilon}}$  /* Adaptive coefficient update */
11  $U, S, V, S_{\mathcal{V}}, S_{\mathcal{K}} \leftarrow \text{truncation}(\hat{S}, \hat{S}_{\mathcal{V}}, \hat{S}_{\mathcal{K}}, \hat{U}, \hat{V}; \tau)$ 

```

We apply the Adam bias correction at iteration n to the low-rank moments, i.e.,

$$\check{S}_{\mathcal{V}} = \frac{\hat{S}_{\mathcal{V}}^n}{1 - \beta_1^n}, \quad \text{and} \quad \check{S}_{\mathcal{K}} = \frac{\hat{S}_{\mathcal{K}}^n}{1 - \beta_2^n},$$

and update steps for the coefficient S , i.e., $\hat{S}^1 = \bar{S} - \lambda \frac{\check{S}_{\mathcal{V}}}{\sqrt{\hat{S}_{\mathcal{K}} + \epsilon}}$.

The resulting method is summarized in Algorithm 2. We wish to remark that an extension to Tucker tensors of this algorithm is straightforward and follows the extension of the sgd-based DLRT method from matrices in [24] to tensors [36]. Furthermore, extension to AdamW is straightforward: The regularization term is added to \hat{S} directly instead of being combined with the gradient for the moment updates.

Computational and Memory Efficiency

We briefly analyze the computational and memory efficiency of 1) the low-rank Heavy Ball method and 2) the low-rank Adam method. To update a matrix $W \in \mathbb{R}^{n \times n}$, the full-rank (baseline) Heavy Ball method requires $\mathcal{O}(3n^2)$ floats to store the weight W , its gradient $\nabla_W \mathcal{L}$, and the momentum \mathcal{V} . The computational cost is of the same order. In contrast, the low-rank Heavy Ball method (see Algorithm 1) requires $\mathcal{O}(2nr + r^2)$ floats to store the low-rank factorization USV^\top , and $\mathcal{O}(2nr + r^2)$ for the gradients $\nabla_U \mathcal{L}, \nabla_V \mathcal{L}, \nabla_S \mathcal{L}$. Since the bases U and V are shared between the weight and momentum, the momentum term requires only $\mathcal{O}(r^2)$ additional floats. The extra computational costs are $\mathcal{O}(nr^2)$ for orthonormalization during basis augmentation and $\mathcal{O}(r^3)$ for truncation, both negligible when $r \ll n$. Similarly, the full-rank Adam/AdamW method requires $\mathcal{O}(4n^2)$ floats to store $W, \nabla_W \mathcal{L}$, and the two momentum terms \mathcal{V}, \mathcal{K} , with comparable compute cost. The low-rank Adam method uses $\mathcal{O}(2nr + r^2)$ for USV^\top and the same for the gradients. The two momentum terms add only $\mathcal{O}(2r^2)$ due to shared bases. The computational cost is computed analogously to that of the low-rank Heavy Ball method.

Table 1: UCM, Cifar10 and Cifar100 benchmark; Low-rank pretraining. Accuracy means and std. devs. of 10 stochastic trainings using AdamW. The LoRA ranks are set up to match the compression rate of the results of Algorithm 2. Algorithm 2 achieves higher accuracy at higher compression rates across all benchmarks, compared to DLRT[24] w/o momentum term projection and LoRA-based pretraining w/ momentum terms.

		UCM Data		Cifar10 Data		Cifar100 Data	
		Acc [%]	c.r. [%]	Acc [%]	c.r. [%]	Acc [%]	c.r. [%]
VGG16	Baseline	94.40±0.72	0.0	89.82±0.45	0.0	65.21±0.37	0.0
	Algorithm 2	94.61±0.35	95.84	89.49±0.58	95.30	64.58±0.46	95.54
	DLRT w/o proj.	89.32±0.93	93.56	85.01±0.28	94.84	60.48±0.27	98.71
	LoRA pretrain	90.64±2.27	93.57	88.43±0.23	94.80	61.63±0.46	96.58
VGG11	Baseline	94.23±0.71	0.0	88.34±0.49	0.0	63.13±0.41	0.0
	Algorithm 2	93.70±0.71	94.89	88.13±0.56	95.13	60.84±0.40	95.08
	DLRT w/o proj.	88.23±0.90	90.35	81.98±0.25	97.08	61.59±0.25	95.99
	LoRA pretrain	90.14±2.56	94.72	86.63±0.29	94.57	59.54±0.40	94.78
ViT-B/16	Baseline	96.72±0.36	0.0	95.42±0.35	0.0	90.34±0.44	0.0
	Algorithm 2	96.38±0.60	86.7	95.39±0.41	83.42	88.48±0.53	75.38
	DLRT w/o proj.	78.94±0.50	84.91	91.95±0.50	84.95	75.09±0.53	75.83
	LoRA pretrain	86.54±2.91	84.94	94.10±0.56	80.78	76.76±0.53	74.86

Extension to Tensor-valued layers

The proposed momentum-based low-rank optimizer is directly extendable to tensor-valued neural network layers, e.g. convolutional layers. To that end, we remark that a, e.g. 2d, convolution can be formulated as an operation on an order four tensor $\mathbf{W} \in \mathbb{R}^{d_i \times d_o \times s_w \times s_h}$, where d_i and d_o are the channels of the input and output data, and s_w, s_h is the width and height of the sliding window of the convolution acting on the spatial dimensions s, h of the input image $x \in \mathbb{R}^{s \times h \times d_i}$. Consider a low-rank Tucker factorization of the weight, i.e. $\mathbf{W} = \mathbf{C} \times_{i=1}^4 U_i$, with core tensor $\mathbf{C} \in \mathbb{R}^{r_1 \times r_2 \times r_3 \times r_4}$ and $U_i \in \mathbb{R}^{n_i \times r_i}$ with $n_i \in \{d_i, d_o, s_w, s_h\}$. Using the extension of the DLRT method to Tucker tensors [35] and applying Algorithm 1, respectively Algorithm 2 to the tensor update yields the desired method.

5 Numerical Results

Low-Rank pretraining and compression We conduct experiments on three standard image classification benchmarks: the University of California, Merced (UCM) Land Use Dataset, CIFAR-10, and CIFAR-100. Details of the datasets and preprocessing are provided in Section 10. We evaluate performance across three network architectures, VGG16 and VGG11, and the ViT-B/16 Vision Transformer. The convolutional VGG11 and VGG16 networks are selected to validate the performance of Algorithm 2 on tensor-valued layers, here given by the convolutional layers. We use the low-rank Tucker tensor format to compress and train the convolutions; for details, we refer to [26, 35].

Our primary baseline is *full-rank training*, where all model parameters are updated without any structural constraints. We compare this against 1) the low-rank fine-tuning strategy introduced in Algorithm 2 2) naive application of DLRT without the projection of the momentum terms, and 3) simultaneous direct application of the Adam optimizer on the low-rank factors U, S, V , as typically done in LoRA [12], a low-rank adaptation technique originally designed for parameter-efficient fine-tuning of large transformers.

For LoRA-based experiments, we calibrate the per-layer rank hyperparameters to match the overall *compression ratio* achieved by Algorithm 2, ensuring a fair comparison at fixed parameter budgets. The compression ratio is defined as: $\text{c.r.} = \left(1 - \frac{\#\text{params low-rank model}}{\#\text{params baseline model}}\right) \times 100$.

We initialize all the convolutional networks with PyTorch Imagenet1K weights and ViT-B/16 with Huggingface Imagenet21K weights. Stochasticity during training stems from randomized mini-batching. For each experiment, we report the mean performance across 10 independent training runs with different random seeds. We observe in Table 1 that Algorithm 2 matches the validation accuracy of the baseline network in most test-cases, and surpasses the baseline in e.g. UCM/VGG16

Table 2: DeBERTaV3-base fine-tuning on GLUE. We compare with full fine-tuning (Full FT), Houslyby adapter [11] (HAdapter), Pfeiffer adapter [20] (PAdapter), LoRA [12], AdaLoRA [37], GeoLoRA[23], DoRA [18], LoRA+[7], and Bitfit[34]. We report target metrics and computational performance (higher is better) for the median of 5 runs using different random seeds. Best results per dataset are shown in bold. Results for BitFit, HAdapter, and PAdapter were taken from [37]. "AdaLoRa matched" has the rank budget adapted to approximately match the final parameter count of Algorithm 2.

Method (# Params)	SST-2 (Acc)	CoLA (Mcc)	QQP (F1)	QNLI (Acc)	RTE (Acc)	MRPC (Acc)	STS-B (Corr)	Mean
Full FT (184M)	95.63	69.19	89.80	94.03	83.75	89.46	91.60	87.63
BitFit (0.1M)	94.84	66.96	84.95	92.24	78.70	87.75	91.35	85.25
HAdapter (1.22M)	95.53	68.64	89.27	94.11	84.48	89.95	91.48	87.63
PAdapter (1.18M)	95.61	68.77	89.40	94.29	85.20	89.46	91.54	87.75
LoRA $r=8$ (1.33M)	95.29	68.57	90.61	93.91	85.50	89.75	89.10	87.53
LoRA+ $r=8$ (1.33M)	95.37	69.22	90.82	93.96	85.50	89.55	88.07	87.49
DoRA $r=8$ (1.33M)	94.30	68.50	90.71	94.31	85.05	89.32	91.38	87.65
AdaLoRA $r_f = 8$ (1.27M)	95.64	68.76	90.65	94.11	86.00	89.44	91.41	88.00
AdaLoRA, matched	95.64 (1.27M)	68.59 (1.07M)	90.48 (0.72M)	93.93 (0.72M)	85.92 (1.16M)	88.21 (0.74M)	90.91 (0.74M)	87.66 (0.91M)
GeoLoRA	95.98 (1.17M)	69.03 (0.98M)	90.53 (0.69M)	94.23 (0.70M)	85.93 (1.19M)	90.10 (0.75M)	91.58 (0.71M)	88.19 (0.88M)
Algorithm 2	96.02 (1.11M)	69.58 (1.01M)	90.62 (0.76M)	94.02 (0.70M)	88.67 (1.19M)	90.84 (0.76M)	91.51 (0.73M)	88.75 (0.89M)

while achieving compression rates of up to 95%. We point out that a naive implementation of DLRT without the proposed adaptation of the optimizer states causes performance drops of 5 to 13%. LoRA also struggles to achieve high accuracy at the prescribed compression rates.

GLUE with low-rank finetuning of DeBERTa. To assess the effectiveness of Algorithm 2, we fine-tune the 183M parameter DeBERTaV3-base transformer model [8] on the GLUE benchmark suite [30]. The corresponding results are summarized in Table 2. Additional implementation details, including the experimental setup and hyperparameter configurations, can be found in Appendix 10.2. Overall, Algorithm 2 consistently outperforms competing methods, especially other rank adaptive methods as GeoLoRA [23] and AdaLoRA [37], on most tasks, achieving stronger validation metrics. The required number of trainable parameters is substantially lower than the compared fixed-rank methods. The average score is higher than the reference methods, and the average parameter count for the finetuning tasks is lower than the next best method, which is GeoLoRA.

Pretraining from scratch of ViT-small on Cifar10 We consider a compact Vision Transformer architecture for the CIFAR-10 dataset, see Section 10.1 for details on training and architecture. We compare baseline full-rank training with LoRA pretraining, Algorithm 2, and the naive implementation of Adam with DLRT [24]. Instead of low-rank finetuning, we pretrain the network from scratch and initialize the weights with a normal distribution. The low-rank methods factorize the fully-connected layers, while keeping the attention layers, which are typically high-rank, in baseline format. The LoRA rank is chosen to match the final compression rate of the rank adaptive naive DLRT and Algorithm 2 method, which achieves a compression rate of 67%. Remark that the compression rate is lower, since the attention matrices remain full-rank.

The goal of this test is to compare the long-term convergence behavior of all four methods, presented in Figure 2. We observe that Algorithm 2 and standard LoRA pretraining first converge faster than the baseline training. The non-orthogonal bases A, B of LoRA and the corresponding non-orthogonal projection onto the low-rank manifold cause LoRA to plateau, whereas Algorithm 2 achieves lower loss values and higher validation accuracies, even surpassing the full-rank baseline in this test case. Naive implementation of DLRT with the Adam optimizer causes a more than 10% reduction in validation accuracy and slower convergence.

6 Conclusion

We introduced a principled and provably robust framework for momentum-based low-rank optimization that is both rank-adaptive and jointly compresses weights, gradients, and optimizer states. Our analysis reveals that the proposed method is resilient to the conditioning of the training problem, while maintaining fidelity to full-rank momentum trajectories. Through extensive experiments on pretraining, transfer learning, and finetuning, we demonstrate that our approach consistently achieves stronger generalization performance under tight parameter budgets, outperforming existing low-rank

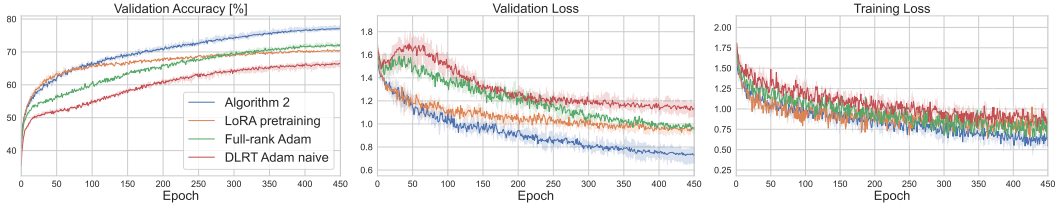


Figure 2: ViT-small on Cifar10, pretrained from scratch in low-rank and full-rank baseline format for 450 epochs. Median trajectory over 5 runs. Algorithm 2 and LoRA pretraining initially converge faster than the full-rank baseline. Algorithm 2 achieves lower loss and higher validation accuracy than LoRA, even surpassing the baseline. A naive DLRT implementation with Adam leads to slower convergence and over 10% drop in validation accuracy.

techniques. These results position our method as a strong foundation for efficient deep learning, offering a scalable and theoretically grounded alternative to full-rank training across diverse regimes.

The accomplished faster convergence and higher compression of the optimizer states during training enable broader applications of machine learning on resource-constrained devices. Furthermore, the method is computationally efficient and scalable. These achievements also enhance computational and memory efficiency, positively impacting society.

Funding Acknowledgements

This material is based upon work supported by the Laboratory Directed Research and Development Program of Oak Ridge National Laboratory (ORNL), managed by UT-Battelle, LLC for the U.S. Department of Energy under Contract No. De-AC05-00OR22725.

This manuscript has been authored by UT-Battelle, LLC under Contract No. DE-AC05-00OR22725 with the U.S. Department of Energy. The United States Government retains and the publisher, by accepting the article for publication, acknowledges that the United States Government retains a non-exclusive, paid-up, irrevocable, world-wide license to publish or reproduce the published form of this manuscript, or allow others to do so, for United States Government purposes. The Department of Energy will provide public access to these results of federally sponsored research in accordance with the DOE Public Access Plan(<http://energy.gov/downloads/doe-public-access-plan>).

References

- [1] G. Ceruti, J. Kusch, and C. Lubich. A rank-adaptive robust integrator for dynamical low-rank approximation. *BIT Numerical Mathematics*, pages 1–26, 2022.
- [2] G. Ceruti, J. Kusch, and C. Lubich. A parallel rank-adaptive integrator for dynamical low-rank approximation. *SIAM Journal on Scientific Computing*, 46(3):B205–B228, 2024.
- [3] D. Coquelin, K. Flügel, M. Weiel, N. Kiefer, C. Debus, A. Streit, and M. Götz. Harnessing orthogonality to train low-rank neural networks. In *ECAI 2024*, pages 2106–2113. IOS Press, 2024.
- [4] M. Courbariaux, I. Hubara, D. Soudry, R. El-Yaniv, and Y. Bengio. Binarized Neural Networks: Training Deep Neural Networks with Weights and Activations constrained to +1 or -1. *arXiv:1602.02830*, 2016.
- [5] R. J. George, D. Pitt, J. Zhao, J. Kossaifi, C. Luo, Y. Tian, and A. Anandkumar. Tensor-GaLore: Memory-Efficient Training via Gradient Tensor Decomposition, 2025.
- [6] Y. Guo, A. Yao, and Y. Chen. Dynamic Network Surgery for Efficient DNNs. *Advances in neural information processing systems*, 29, 2016.
- [7] S. Hayou, N. Ghosh, and B. Yu. LoRA+: Efficient Low Rank Adaptation of Large Models, 2024.
- [8] P. He, J. Gao, and W. Chen. DeBERTav3: Improving DeBERTa using ELECTRA-Style Pre-Training with Gradient-Disentangled Embedding Sharing, 2023.
- [9] Y. He, X. Zhang, and J. Sun. Channel Pruning for Accelerating Very Deep Neural Networks. In *Proceedings of the IEEE international conference on computer vision*, pages 1389–1397, 2017.
- [10] A. Hnatiuk, J. Kusch, L. Kusch, N. R. Gauger, and A. Walther. Stochastic Aspects of Dynamical Low-Rank Approximation in the Context of Machine Learning. *Optimization Online*, 2024.
- [11] N. Hounsby, A. Giurgiu, S. Jastrzebski, B. Morrone, Q. De Laroussilhe, A. Gesmundo, M. Attariyan, and S. Gelly. Parameter-Efficient Transfer Learning for NLP. In K. Chaudhuri and R. Salakhutdinov, editors, *Proceedings of the 36th International Conference on Machine Learning*, volume 97 of *Proceedings of Machine Learning Research*, pages 2790–2799. PMLR, 09–15 Jun 2019.
- [12] E. J. Hu, Y. Shen, P. Wallis, Z. Allen-Zhu, Y. Li, S. Wang, L. Wang, and W. Chen. LoRA: Low-Rank Adaptation of Large Language Models. *arXiv preprint arXiv:2106.09685*, 2021.
- [13] M. Khodak, N. Tenenholz, L. Mackey, and N. Fusi. Initialization and Regularization of Factorized Neural Layers. In *International Conference on Learning Representations*, 2021.
- [14] D. P. Kingma and J. Ba. Adam: A method for stochastic optimization. In Y. Bengio and Y. LeCun, editors, *3rd International Conference on Learning Representations, ICLR 2015, San Diego, CA, USA, May 7-9, 2015, Conference Track Proceedings*, 2015.
- [15] O. Koch and C. Lubich. Dynamical low-rank approximation. *SIAM Journal on Matrix Analysis and Applications*, 29(2):434–454, 2007.
- [16] J. Kusch, S. Schotthöfer, and A. Walter. An Augmented Backward-Corrected Projector Splitting Integrator for Dynamical Low-Rank Training, 2025.
- [17] V. Lialin, S. Muckatira, N. Shivagunde, and A. Rumshisky. ReloRA: High-rank training through low-rank updates. In *The Twelfth International Conference on Learning Representations*, 2024.
- [18] Y. Mao, K. Huang, C. Guan, G. Bao, F. Mo, and J. Xu. DoRA: Enhancing Parameter-Efficient Fine-Tuning with Dynamic Rank Distribution. In L.-W. Ku, A. Martins, and V. Srikumar, editors, *Proceedings of the 62nd Annual Meeting of the Association for Computational Linguistics (Volume 1: Long Papers)*, pages 11662–11675, Bangkok, Thailand, Aug. 2024. Association for Computational Linguistics.

- [19] P. Molchanov, S. Tyree, T. Karras, T. Aila, and J. Kautz. Pruning Convolutional Neural Networks for Resource Efficient Inference. In *International Conference on Learning Representations*, 2017.
- [20] J. Pfeiffer, A. Kamath, A. Rücklé, K. Cho, and I. Gurevych. Adapterfusion: Non-Destructive Task Composition for Transfer Learning, 2021.
- [21] H. Sato. *Riemannian optimization and its applications*, volume 670. Springer, 2021.
- [22] D. Savostianova, E. Zangrando, G. Ceruti, and F. Tudisco. Robust low-rank training via approximate orthonormal constraints. *Advances in Neural Information Processing Systems*, 36:66064–66083, 2023.
- [23] S. Schotthöfer, E. Zangrando, G. Ceruti, F. Tudisco, and J. Kusch. GeoLoRA: Geometric integration for parameter efficient fine-tuning. In *The Thirteenth International Conference on Learning Representations*, 2025.
- [24] S. Schotthöfer, E. Zangrando, J. Kusch, G. Ceruti, and F. Tudisco. Low-rank lottery tickets: finding efficient low-rank neural networks via matrix differential equations. In S. Koyejo, S. Mohamed, A. Agarwal, D. Belgrave, K. Cho, and A. Oh, editors, *Advances in Neural Information Processing Systems*, volume 35, pages 20051–20063. Curran Associates, Inc., 2022.
- [25] S. Schotthöfer and M. P. Laiu. Federated Dynamical Low-Rank Training with Global Loss Convergence Guarantees, 2024.
- [26] S. Schotthöfer, H. L. Yang, and S. Schnake. Dynamical low-rank compression of neural networks with robustness under adversarial attacks, 2025.
- [27] N. Shazeer and M. Stern. Adafactor: Adaptive Learning Rates with Sublinear Memory Cost. In J. Dy and A. Krause, editors, *Proceedings of the 35th International Conference on Machine Learning*, volume 80 of *Proceedings of Machine Learning Research*, pages 4596–4604. PMLR, 10–15 Jul 2018.
- [28] S. P. Singh, G. Bachmann, and T. Hofmann. Analytic insights into structure and rank of neural network Hessian maps. In *Advances in Neural Information Processing Systems*, volume 34, 2021.
- [29] M. Valipour, M. Rezagholizadeh, I. Kobzyev, and A. Ghodsi. Dylora: Parameter Efficient Tuning of Pre-trained Models using Dynamic Search-Free Low-Rank Adaptation, 2023.
- [30] A. Wang, A. Singh, J. Michael, F. Hill, O. Levy, and S. R. Bowman. Glue: A Multi-Task Benchmark and Analysis Platform for Natural Language Understanding, 2019.
- [31] H. Wang, S. Agarwal, and D. Papailiopoulos. Pufferfish: Communication-efficient models at no extra cost. *Proceedings of Machine Learning and Systems*, 3:365–386, 2021.
- [32] J. Wu, C. Leng, Y. Wang, Q. Hu, and J. Cheng. Quantized Convolutional Neural Networks for Mobile Devices. In *Proceedings of the IEEE conference on computer vision and pattern recognition*, pages 4820–4828, 2016.
- [33] Y. Yang and S. Newsam. Bag-of-visual-words and spatial extensions for land-use classification. In *Proceedings of the 18th SIGSPATIAL International Conference on Advances in Geographic Information Systems*, GIS '10, page 270–279, New York, NY, USA, 2010. Association for Computing Machinery.
- [34] E. B. Zaken, S. Ravfogel, and Y. Goldberg. Bitfit: Simple Parameter-efficient Fine-tuning for Transformer-based Masked Language-models, 2022.
- [35] E. Zangrando, S. Schotthöfer, G. Ceruti, J. Kusch, and F. Tudisco. Geometry-aware training of factorized layers in tensor tucker format. In A. Globerson, L. Mackey, D. Belgrave, A. Fan, U. Paquet, J. Tomczak, and C. Zhang, editors, *Advances in Neural Information Processing Systems*, volume 37, pages 129743–129773. Curran Associates, Inc., 2024.

- [36] E. Zangrando, S. Schotthöfer, G. Ceruti, J. Kusch, and F. Tudisco. Rank-adaptive spectral pruning of convolutional layers during training. In *Advances in Neural Information Processing Systems*, 2024.
- [37] Q. Zhang, M. Chen, A. Bukharin, P. He, Y. Cheng, W. Chen, and T. Zhao. AdaLoRA: Adaptive Budget Allocation for Parameter-Efficient Fine-Tuning. In *The Eleventh International Conference on Learning Representations*, 2023.
- [38] J. Zhao, Z. Zhang, B. Chen, Z. Wang, A. Anandkumar, and Y. Tian. GaLore: Memory-Efficient LLM Training by Gradient Low-Rank Projection, 2024.

7 Notation

Table 3: Summary of notation used throughout the paper.

Notation	Definition
Model & Training	
$W_l \in \mathbb{R}^{n_l \times n_{l-1}}$	The weight matrix for layer l .
\mathcal{L}	The loss function.
$\nabla_W \mathcal{L}$	The gradient of the loss with respect to the full matrix W .
λ	The learning rate of stochastic gradient descent.
Low-Rank Factorization	
\mathcal{M}_r	The manifold of matrices of rank r .
$P(W)Z$	Orthogonal projection of a matrix Z onto the tangent space of \mathcal{M}_r at W .
$W = USV^\top$	Low-rank decomposition of W , where U, V are orthonormal.
$U \in \mathbb{R}^{n_l \times r}, V \in \mathbb{R}^{n_{l-1} \times r}$	Orthonormal basis matrices for the column and row spaces.
$S \in \mathbb{R}^{r \times r}$	The core tensor or coefficient matrix.
$\nabla_U \mathcal{L}, \nabla_S \mathcal{L}, \nabla_V \mathcal{L}$	Gradients with respect to the low-rank factors U, S, V .
Momentum Terms (Heavy Ball)	
\mathcal{V}	The momentum term (a full-rank matrix).
$U_V S_V V_V^\top$	Low-rank decomposition of the momentum term.
$S_V \in \mathbb{R}^{r \times r}$	The coefficient matrix for the momentum term.
γ	The momentum decay parameter.
Momentum Terms (Adam)	
\mathcal{V}	The momentum term (a full-rank matrix).
$U_V S_V V_V^\top$	Low-rank decomposition of 1st moment term (moving average of gradients).
$S_V \in \mathbb{R}^{r \times r}$	Coefficient matrix for the 1st moment (moving average of gradients).
\mathcal{K}	The momentum term (a full-rank matrix).
$U_K S_K V_K^\top$	Low-rank decomposition of the 2nd moment.
$S_K \in \mathbb{R}^{r \times r}$	Coefficient matrix for the 2nd moment (moving average of squared gradients).
β_1, β_2	Exponential decay rates for the moment estimates.
Algorithm-Specific	
\hat{U}, \hat{V}	Augmented bases after incorporating gradient information.
\bar{S}	Coefficient matrix S projected onto the augmented bases \hat{U}, \hat{V} .
\bar{S}_V, \bar{S}_K	Momentum coefficients projected onto the new augmented bases.
\hat{S}	The final updated coefficient matrix within a single optimization step.
τ, ϑ	Relative and absolute truncation tolerance parameter for rank adaptation.

8 Algorithms

We list the helper functions of Algorithm 1 and Algorithm 1 in Algorithm 3. The baseline (full-rank) Adam method is listed in Algorithm 4.

9 Numerical Analysis

Theorem 1 (Convergence). *Let $W(t)$ be the solution of (6) and let \mathcal{L} be bounded from below. Then, $W(t)$ converges to a W^* which fulfills the low-rank optimality condition*

$$P(W^*)\nabla_W \mathcal{L}(W^*) = 0. \quad (9)$$

Proof. Let us define the energy as

$$E(t) := \mathcal{L}(W(t)) + \frac{1}{2} \|\mathcal{V}(t)\|^2.$$

Algorithm 3: The functions `basis_augmentation`, and truncation of the used algorithms.

```

1 def basis_augmentation( $B$ : old basis,  $G_B$ : basis dynamics):
2    $\widehat{B} \leftarrow \text{ortho}([G_B \mid B])$           /* orthonormalization, e.g. Gram-Schmidt */
3   return  $\widehat{B}$ 
4 def truncation( $\widehat{S}$ : augmented coefficient,  $\widehat{S}_V$ : augmented momentum,  $\widehat{U}$ : augmented basis,
5    $\widehat{V}$ : augmented co-basis ):
6    $P_{r_1}, \Sigma_{r_1}, Q_{r_1} \leftarrow \text{truncated svd}(\widehat{S})$  with threshold  $\vartheta$  to new rank  $r_1$ 
7    $U \leftarrow \widehat{U}P_{r_1}; V \leftarrow \widehat{V}Q_{r_1}$           /* Basis update */
8    $S \leftarrow \Sigma_{r_1}; S_V \leftarrow U^\top \widehat{U} \widehat{S}_V \widehat{V}^\top V$           /* Coefficient update */
9   return  $U, S, V, S_V$ 
10 def truncation( $\widehat{S}$ : augmented coefficient,  $\widehat{S}_V$ : augmented momentum,  $\widehat{S}_K$ : augmented 2nd
11   momentum,  $\widehat{U}$ : augmented basis,  $\widehat{V}$ : augmented co-basis ):
12    $P_{r_1}, \Sigma_{r_1}, Q_{r_1} \leftarrow \text{truncated svd}(\widehat{S})$  with threshold  $\vartheta$  to new rank  $r_1$ 
13    $U \leftarrow \widehat{U}P_{r_1}; V \leftarrow \widehat{V}Q_{r_1}$           /* Basis update */
14    $S \leftarrow \Sigma_{r_1}; S_V \leftarrow U^\top \widehat{U} \widehat{S}_V \widehat{V}^\top V; \widehat{S}_K \leftarrow \left( U^\top \widehat{U} \sqrt{S_K} \widehat{V}^\top V \right)^2$  /* Coefficient update */
15   return  $U, S, V, S_V, S_K$ 

```

Algorithm 4: Single iteration of the (full-rank version of) Adam.

Input : Initial parameter vector $W \in \mathbb{R}^{n \times n}$;
 \mathcal{V} : Initial 1st moment;
 \mathcal{K} : Initial 2nd moment;
Gradient $g = \nabla_W \mathcal{L}(W)$;
 λ : learning rate;
 β_1, β_2 : Adam momentum parameters;
 ϵ : Small stability constant.

```

1 Evaluate  $\mathcal{L}(W)$ 
2  $g \leftarrow \nabla_W \mathcal{L}(W)$           /* Compute gradient */
3  $\mathcal{V} \leftarrow \beta_1 \mathcal{V} + (1 - \beta_1)g$           /* 1st moment estimate */
4  $\mathcal{K} \leftarrow \beta_2 \mathcal{K} + (1 - \beta_2)g^2$           /* 2nd moment estimate (element-wise square) */
5  $\hat{\mathcal{V}} \leftarrow \frac{\mathcal{V}}{1 - \beta_1^t}, \hat{\mathcal{K}} \leftarrow \frac{\mathcal{K}}{1 - \beta_2^t}$           /* Bias correction */
6  $W \leftarrow W - \lambda \frac{\hat{\mathcal{V}}}{\sqrt{\hat{\mathcal{K}} + \epsilon}}$           /* Parameter update */

```

The time derivative is given by

$$\begin{aligned} \dot{E}(t) &:= \langle \nabla_W \mathcal{L}(W(t)), \dot{W}(t) \rangle + \langle \mathcal{V}(t), \dot{\mathcal{V}}(t) \rangle \\ &= \langle \nabla_W \mathcal{L}(W(t)), P(W(t))\mathcal{V}(t) \rangle + \langle \mathcal{V}(t), -\gamma \mathcal{V}(t) - P(W(t))\nabla_W \mathcal{L}(W(t)) \rangle. \end{aligned}$$

Since P is self-adjoint this directly gives

$$\begin{aligned} \dot{E}(t) &= \langle P(W(t))\nabla_W \mathcal{L}(W(t)), \mathcal{V}(t) \rangle + \langle \mathcal{V}(t), -\gamma \mathcal{V}(t) - P(W(t))\nabla_W \mathcal{L}(W(t)) \rangle \\ &= -\gamma \|\mathcal{V}(t)\|^2. \end{aligned}$$

Hence, if \mathcal{L} is bounded from below, this means that $\lim_{t \rightarrow \infty} E(t) = E_\infty$ with E_∞ finite and

$$E_\infty = E(0) - \gamma \int_0^\infty \|\mathcal{V}(t)\|^2 dt.$$

This implies that $\lim_{t \rightarrow \infty} \mathcal{V}(t) = 0$ and thus $\lim_{t \rightarrow \infty} \dot{W}(t) = \lim_{t \rightarrow \infty} P(W(t))\mathcal{V}(t) = 0$. Hence, since $\mathcal{V}(t), W(t)$ converge to a steady state and $\lim_{t \rightarrow \infty} \mathcal{V}(t) = 0$, the evolution equation for \mathcal{V} gives $P(W(t))\nabla_W \mathcal{L}(W(t)) = 0$ as $t \rightarrow \infty$. \square

We can obtain a similar, but not equivalent, result when solving a low-rank gradient flow of the form (8) instead:

Theorem 2 (Convergence of low-rank factors). *The low-rank gradient flow*

$$\dot{U}_{\mathcal{V}} = -(I - U_{\mathcal{V}}U_{\mathcal{V}}^{\top})\nabla_W \mathcal{L}V_{\mathcal{V}}S_{\mathcal{V}}^{-1}, \quad (10a)$$

$$\dot{V}_{\mathcal{V}} = -(I - V_{\mathcal{V}}V_{\mathcal{V}}^{\top})\nabla_W \mathcal{L}^{\top}U_{\mathcal{V}}S_{\mathcal{V}}^{-\top}, \quad (10b)$$

$$\dot{S}_{\mathcal{V}} = -\gamma S_{\mathcal{V}} - U_{\mathcal{V}}^{\top}\nabla_W \mathcal{L}V_{\mathcal{V}}, \quad (10c)$$

fulfills

$$\dot{\mathcal{V}} = -\gamma\mathcal{V} - P(\mathcal{V})\nabla_W \mathcal{L}.$$

Proof. By the product rule we have

$$\begin{aligned} \dot{\mathcal{V}} &= \dot{U}_{\mathcal{V}}S_{\mathcal{V}}V_{\mathcal{V}}^{\top} + U_{\mathcal{V}}\dot{S}_{\mathcal{V}}V_{\mathcal{V}}^{\top} + U_{\mathcal{V}}S_{\mathcal{V}}\dot{V}_{\mathcal{V}}^{\top} \\ &= -\gamma\mathcal{V} - (I - U_{\mathcal{V}}U_{\mathcal{V}}^{\top})\nabla_W \mathcal{L}V_{\mathcal{V}}V_{\mathcal{V}}^{\top} - U_{\mathcal{V}}U_{\mathcal{V}}^{\top}\nabla_W \mathcal{L}V_{\mathcal{V}}V_{\mathcal{V}}^{\top} - U_{\mathcal{V}}U_{\mathcal{V}}^{\top}\nabla_W \mathcal{L}(I - V_{\mathcal{V}}V_{\mathcal{V}}^{\top}) \\ &= -\gamma\mathcal{V} - P(\mathcal{V})\nabla_W \mathcal{L}. \end{aligned} \quad (11)$$

□

Theorem 3 (Error-bound). *For an integer k , let $t = k\lambda$. Let $W(t)$ be the solution of (6), and let W_t^r , \mathcal{V}_t be the factorized low-rank solution after k steps with Algorithm 1. Assume that for any $Z \in \mathcal{M}_r$ in a neighborhood of W_t^r , we have $\|(I - P(Z))\nabla \mathcal{L}(Z)\| < \varepsilon$ and $\|\widehat{U}_t\widehat{U}_t^{\top}\mathcal{V}_t\widehat{V}_t\widehat{V}_t^{\top} - U_tU_t^{\top}\mathcal{V}_tV_tV_t^{\top}\| \leq \widehat{\vartheta}$, where $\|\cdot\|$ denotes the Frobenius norm. Moreover, assume that the gradient is bounded and Lipschitz continuous. Then,*

$$\|W(t) - W_t^r\| \leq c_1\varepsilon + c_2\lambda + c_3\widehat{\vartheta}/\lambda + c_4\widehat{\vartheta}/\lambda, \quad (12)$$

where the constants c_1, c_2, c_3 are independent of singular values of S^{-1} and $S_{\mathcal{V}}^{-1}$.

Proof. We start by bounding the local error. That is, we assume that $W(t_0) = W_0^r$ and $\mathcal{V}(t_0) = \mathcal{V}_0^r$, where \mathcal{V}_0^r is the momentum of the low-rank method. By definition of \widehat{U} we have $(I - \widehat{U}\widehat{U}^{\top})\mathcal{V}(t_0) = 0$ and thus

$$\|(I - \widehat{U}\widehat{U}^{\top})\mathcal{V}(t)\| \leq \int_{t_0}^t \|(I - \widehat{U}\widehat{U}^{\top})(\gamma\mathcal{V}(s) + P(W(s))\nabla_W \mathcal{L}(W(s)))\| ds.$$

Using the boundedness of normal components and a Taylor expansion around t_0 gives for $s \in [t_0, t_1]$

$$\begin{aligned} P(W(s))\nabla_W \mathcal{L}(W(s)) &= \nabla_W \mathcal{L}(W(s)) + O(\varepsilon) = \nabla_W \mathcal{L}(W(t_0)) + O(\lambda + \varepsilon) \\ &= P(W(t_0))\nabla_W \mathcal{L}(W(t_0)) + O(\lambda + \varepsilon). \end{aligned} \quad (13)$$

Hence, with $\mathcal{V}(s) = \mathcal{V}(t_0) + O(\lambda + \varepsilon)$,

$$\begin{aligned} \|(I - \widehat{U}\widehat{U}^{\top})\mathcal{V}(t)\| &\leq \lambda\|(I - \widehat{U}\widehat{U}^{\top})(\gamma\mathcal{V}(t_0) + P(W(t_0))\nabla_W \mathcal{L}(W(t_0)))\| + O(\lambda^2 + \lambda\varepsilon) \\ &= \lambda\|(I - \widehat{U}\widehat{U}^{\top})\nabla_W \mathcal{L}(W(t_0))V_0V_0^{\top}\| + O(\lambda^2 + \lambda\varepsilon). \end{aligned}$$

By construction of \widehat{U} we have $0 = (I - \widehat{U}\widehat{U}^{\top})\nabla_U \mathcal{L}(W(t_0)) = (I - \widehat{U}\widehat{U}^{\top})\nabla_W \mathcal{L}(W(t_0))V_0$, hence

$$\|(I - \widehat{U}\widehat{U}^{\top})\mathcal{V}(t)\| \leq O(\lambda^2 + \lambda\varepsilon).$$

From this, we directly conclude

$$\|(I - \widehat{U}\widehat{U}^{\top})W(t_1)\| = \|(I - \widehat{U}\widehat{U}^{\top})(W(t_0) + \int_{t_0}^{t_1} \mathcal{V}(s) ds)\| = O(\lambda^3 + \lambda^2\varepsilon).$$

An analogous derivation for the co-range gives

$$\begin{aligned} \|W(t_1) - \widehat{U}\widehat{U}^{\top}W(t_1)\widehat{V}\widehat{V}^{\top}\| &\leq \|(I - \widehat{U}\widehat{U}^{\top})W(t_1)\| + \|W(t_1)(I - \widehat{V}\widehat{V}^{\top})\| \\ &= O(\lambda^3 + \lambda^2\varepsilon). \end{aligned}$$

Next, we need to bound

$$\|\widehat{U}\widehat{U}^\top W(t_1)\widehat{V}\widehat{V}^\top - \widehat{U}\widehat{S}^1\widehat{V}^\top\| \leq \|\widehat{U}^\top W(t_1)\widehat{V} - \widehat{S}^1\|. \quad (14)$$

We note that from (13) we have with $W_0 := W(t_0)$ and $\mathcal{V}_0 := \mathcal{V}(t_0)$

$$\begin{aligned} \widehat{U}^\top W(t_1)\widehat{V} &= \widehat{U}^\top (W_0 + \lambda(1-\gamma)\mathcal{V}_0 - \lambda^2 P(W_0)\nabla_W \mathcal{L}(W_0))\widehat{V} + O(\lambda^2 + \lambda\varepsilon) \\ &= \bar{S} - \lambda\gamma\bar{S}_\mathcal{V} - \lambda\widehat{U}^\top \nabla_W \mathcal{L}(W_0)\widehat{V} + O(\lambda^2 + \lambda\varepsilon), \end{aligned}$$

where $\bar{S} = \widehat{U}^\top W_0 \widehat{V}$ and $\bar{S}_\mathcal{V} = \widehat{U}^\top \mathcal{V}_0 \widehat{V}$. By definition of the S -update of Algorithm 2 we have

$$\widehat{S}^1 = \bar{S} + \lambda(1-\gamma)\bar{S}_\mathcal{V} - \lambda^2 \nabla_{\bar{S}} \mathcal{L}(\widehat{U}\bar{S}\widehat{V}^\top).$$

Thus, since $\nabla_{\bar{S}} \mathcal{L}(\widehat{U}\bar{S}\widehat{V}^\top) = U^\top \nabla_W \mathcal{L}(W_0)\widehat{V}$ we have $\|\widehat{U}^\top W(t_1)\widehat{V} - \widehat{S}^1\| = O(\lambda^2 + \lambda\varepsilon)$ and therefore the local error is bounded by

$$\begin{aligned} \|W(t_1) - W_1^r\| &\leq \|W(t_1) - \widehat{U}\widehat{U}^\top W(t_1)\widehat{V}\widehat{V}^\top\| + \|\widehat{U}\widehat{U}^\top W(t_1)\widehat{V}\widehat{V}^\top - \widehat{U}\widehat{S}^1\widehat{V}^\top\| \\ &= O(\lambda^2 + \lambda\varepsilon). \end{aligned}$$

From the truncation tolerance ϑ , the bound on the truncation of \mathcal{V} , and the stability of the exact flow, we can obtain the desired error bound for the global error using Lady Winderemere's fan. \square

We remark, that we can always ensure that condition $\|\widehat{U}_t \widehat{U}_t^\top \mathcal{V}_t \widehat{V}_t \widehat{V}_t^\top - U_t U_t^\top \mathcal{V}_t V_t V_t^\top\| \leq \widehat{\vartheta}$, is fulfilled for a user determined $\widehat{\vartheta}$, e.g. $\widehat{\vartheta} = \vartheta$, by increasing the new rank r_1 in the truncation step of Algorithm 3 if necessary.

10 Details to the numerical experiments of this work

10.1 UCM and Cifar Benchmarks

10.1.1 Network architecture and training details

In this paper, we use the pytorch implementation for neural network training. We take pretrained weights from the imagenet1k dataset as initialization, except for the long-term training study using ViT-small, which is randomly initialized. The data-loader randomly samples a batch for each batch-update which is the only source of randomness in our training setup. Below is an overview of the used network architectures

- VGG16 is a deep convolutional neural network architecture that consists of 16 layers, including 13 convolutional layers and 3 fully connected layers.
- VGG11 is a convolutional neural network architecture similar to VGG16 but with fewer layers, consisting of 11 layers: 8 convolutional layers and 3 fully connected layers. It follows the same design principle as VGG16, using small 3x3 convolution filters and 2x2 max-pooling layers.
- ViTt-B/16 is a Vision Transformer with 16×16 patch size, a deep learning architecture that leverages transformer models for image classification tasks.
- ViT-small is a compact vision transformer with patch size 8×8 , and an embedding dimension of 512. The model comprises six attention layers, each equipped with two heads, followed by a ResNet block and a dropout layer.

The full training setup is described in Table 4. We train DLRT with the same hyperparameters as the full-rank baseline models. It is known [23] that DLRT methods are robust w.r.t. common hyperparameters as learning rate, and batch-size, and initial rank. The truncation tolerance τ is chosen per an initial parameter study. These values are similar to default values reported in recent literature [25, 26, 28]. In general, there is a trade-off between target compression ratio and accuracy, as illustrated e.g. in [24] for matrix-valued and [28] for tensor-valued (CNN) layers.

10.1.2 UCM Data

The UC Merced (UCM) Land Use Dataset [33] is a standard benchmark in remote sensing and computer vision. It consists of 2,100 high-resolution aerial RGB images, each of size 256×256 pixels, organized into 21 land use classes with 100 images per class.

Table 4: Training hyperparameters for the UCM, Cifar10 and Cifar100 Benchmark. The first set hyperparameters apply to both DLRT and baseline training, and we train DLRT with the same hyperparameters as the full-rank baseline models. The second set of hyper-parameters is specific to DLRT. The DLRT hyperparameters are selected by an initial parameter sweep. We choose the DLRT truncation tolerance relative to the Frobenius norm of \hat{S} , i.e. $\vartheta = \tau \|\hat{S}\|_F$, as suggested in [24].

Hyperparameter	VGG16	VGG11	ViT-16b	ViT-small
Batch Size (UCM)	16	16	16	n/a
Batch Size (Cifar10, Cifar100)	128	128	128	256
Learning Rate	0.001	0.001	0.001	0.0001
Number of Epochs (UCM, Cifar10)	20	20	5	450
Number of Epochs (Cifar100)	30	30	20	n/a
L2 regularization	0	0	0.001	1e-2
Optimizer	AdamW	AdamW	AdamW	Adam
DLRT rel. truncation tolerance τ	0.1	0.05	0.08	0.05
Initial Rank	150	150	150	200

We normalize the training and validation data using channel-wise means [0.485, 0.456, 0.406] and standard deviations [0.229, 0.224, 0.225]. Convolutional neural networks (CNNs) are applied directly to the original 256×256 image resolution. For the Vision Transformer (ViT), the input images are resized to 224×224 pixels within the data pipeline.

10.1.3 CIFAR-10 Data

The CIFAR-10 dataset comprises 60,000 RGB images of size 32×32 pixels, uniformly distributed across 10 object classes.

We apply standard data augmentation techniques to the training set, including random horizontal flipping followed by normalization with mean [0.4914, 0.4822, 0.4465] and standard deviation [0.2470, 0.2435, 0.2616]. The test set is only normalized. The same augmentation strategy is applied to CIFAR-100, using mean [0.5071, 0.4867, 0.4408] and standard deviation [0.2673, 0.2564, 0.2762].

CNNs are trained on the original 32×32 resolution, while ViT models receive images resized to 224×224 through the data pipeline.

10.2 GLUE Benchmark

10.2.1 Dataset description

We present the benchmark overview in Table 5. We evaluate ALG against several recent fine-tuning

Table 5: Summary of GLUE benchmark tasks

Corpus	Task	#Train	#Dev	#Test	#Label	Metrics
Single-Sentence Classification (GLUE)						
CoLA	Acceptability	8.5k	1k	1k	2	Matthews corr
SST2	Sentiment	67k	872	1.8k	2	Accuracy
Pairwise Text Classification (GLUE)						
MNLI	NLI	393k	20k	20k	3	Accuracy
RTE	NLI	2.5k	276	3k	2	Accuracy
QQP	Paraphrase	364k	40k	391k	2	F1
MRPC	Paraphrase	3.7k	408	1.7k	2	Accuracy
QNLI	QA/NLI	108k	5.7k	5.7k	2	Accuracy
Text Similarity (GLUE)						
STS-B	Similarity	7k	1.5k	1.4k	1	Pearson/Spearman cor

methods on the General Language Understanding Evaluation (GLUE) benchmark [30]. GLUE is

a standard benchmark comprising a diverse set of natural language understanding tasks that assess a model’s ability to comprehend and process human language. It provides a broad evaluation by including tasks covering various linguistic aspects such as entailment, sentiment, and semantic similarity. The benchmark comprises the following nine tasks:

- **CoLA (Corpus of Linguistic Acceptability)**: Determines if a sentence is grammatically acceptable.
- **SST-2 (Stanford Sentiment Treebank)**: A binary sentiment classification task distinguishing between positive and negative sentiment.
- **MRPC (Microsoft Research Paraphrase Corpus)**: Identifies whether two given sentences are paraphrases.
- **STS-B (Semantic Textual Similarity Benchmark)**: Measures the semantic similarity of two sentences on a continuous scale from 1 to 5.
- **QQP (Quora Question Pairs)**: Assesses whether two questions are semantically equivalent.
- **QNLI (Question Natural Language Inference)**: Determines if a context sentence correctly answers a question.
- **RTE (Recognizing Textual Entailment)**: A binary entailment classification task.
- **Specific Focus: MRPC (Microsoft Research Paraphrase Corpus)**

The F1 score, used for evaluation, is computed from the precision P and recall R as follows. The precision P is defined as

$$P := \frac{P_T}{P_T + P_F}, \quad (15)$$

where P_T denotes the number of true positives and P_F the number of false positives. The recall R is given by

$$R := \frac{P_T}{P_T + N_F}, \quad (16)$$

where N_F represents the number of false negatives. The F1 score is then the harmonic mean of P and R :

$$F1 := \frac{2PR}{P + R}. \quad (17)$$

10.2.2 Reference implementations

Full Finetuning (FT): The standard approach in transfer learning, where the model is initialized with pre-trained weights and all parameters are updated via gradient descent.

Bitfit [34]: Finetuning where only the bias terms are updated while all other parameters remain fixed.

Adapter Tuning [11, 20]: Involves inserting two-layer adapter modules within transformer blocks. In [11], adapters are placed between the self-attention and feed-forward modules with a residual connection (denoted HAdapter). In [20], adapters are inserted after the feed-forward and layer normalization modules (denoted PAdapter), following the notation of [37].

LoRA [12]: Applies low-rank additive updates to selected weight matrices, modeled as

$$\mathbf{z} = \sigma \left(W_{\text{pt}} \mathbf{x} + \frac{\alpha}{r} AB^\top \mathbf{x} \right), \quad (18)$$

where $A, B \in \mathbb{R}^{n \times r}$. We apply LoRA to the attention matrices W_q, W_k, W_v , and the feed-forward matrices W_{f_1} and W_{f_2} . Learning rates and optimizers follow the setup in [37], Appendix D–F.

Results for FT, Bitfit, Adapter tuning, and LoRA in Table 2 are reproduced from [37]. The performance of DoRA, LoRA, LoRA+, and AdaLoRA is computed using the HuggingFace implementations of these adapters.

DoRA [18]: A low-rank adapter similar in structure to LoRA, but with normalized AB matrices and an additional magnitude parameter. Unlike LoRA, DoRA initializes the adapter with the pre-trained weights W_0 , rather than zero.

LoRA+ [7]: Differs from LoRA in the assignment of learning rates: separate learning rates are used for A and B , with a fixed ratio $\lambda_B/\lambda_A = 1.1$.

AdaLoRA [37]: Introduces adaptive low-rank updates to selected weight matrices:

$$\mathbf{z} = \sigma \left(W_{\text{pt}}\mathbf{x} + \frac{\alpha}{r}USV^{\top}\mathbf{x} \right), \tag{19}$$

with frozen base weights $W_{\text{pt}} \in \mathbb{R}^{n \times n}$, rank- r adapters $U, V \in \mathbb{R}^{n \times r}$, and scaling matrix $S \in \mathbb{R}^{r \times r}$. The rank is determined using either SVD-based truncation or sensitivity analysis of the singular vectors. AdaLoRA is applied to W_q, W_k, W_v, W_{f_1} , and W_{f_2} with an orthogonality regularization coefficient $\gamma = 0.1$.

When comparing to AdaLoRA, we align the total parameter budget with LoRA by setting the final budget $b^{(T)}$ to 576, and initialize with $b^{(0)} = 1.5 \times b^{(T)}$.

We also compare AdaLoRA using budget schedules obtained via Algorithm 2, ensuring that $b^{(T)}$ approximately matches the parameter count of the final models trained using Algorithm 2.

GeoLoRA [23]: GeoLoRA integrates the projected gradient flow Equation (8) in a parallelizable single-step scheme, including a rank adaptive augmentation-truncation scheme as the proposed method. However, the method is only applicable for stochastic gradient descent, and not yet extended to momentum-based approaches. We use the hyperparameter choices reported in [23].

We use the implementation of [37, Appendix C] to compute the results for the presented reference methods. We set the exponential moving average parameters β_1 and β_2 of AdamW as their pytorch default value. We select the learning rates as denoted in Table 6, selected by an initial hyperparameter sweep.

We implement ALG as similar as possible to the reference models to achieve a fair comparison. That is, we add an adapter of the form $\mathbf{z} = \sigma(W_{\text{pt}}\mathbf{x} + USV^{\top}\mathbf{x})$ to the key W_k , query W_q and value W_v matrices of all attention blocks, and to both feed-forward layers W_{f_1} and W_{f_2} . For each adapter, we employ Algorithm 2 to update the layer weights and ranks.

Table 6: Hyper-parameter setup for the GLUE benchmark, determined by an initial hyperparameter sweep.

Dataset	Learning Rate	Batch Size	# Epochs	τ	init. rank	Adapter dropout	weight decay
RTE	1.2×10^{-3}	32	20	0.075	10	0.01	0.01
QNLI	5×10^{-4}	64	5	0.05	10	0.2	0.01
MRPC	1×10^{-4}	64	5	0.05	10	0.15	0.05
QQP	1×10^{-4}	64	5	0.05	10	0.15	0.05
SST-2	1×10^{-4}	64	10	0.05	10	0.05	0.01
CoLA	5×10^{-4}	32	25	0.05	10	0.1	0.01
STS-B	1×10^{-3}	128	30	0.05	10	0.05	0.1

10.3 Computational hardware

All experiments in this paper are computed using workstation GPUs. Each training run used a single GPU. Specifically, we have used 5 NVIDIA RTX A6000, and 3 NVIDIA RTX 4090.

The estimated time for one experimental run depends mainly on the data-set size and neural network architecture. For training, and validation testing we estimate 30 minutes on one GPU for one run.